

We are IntechOpen, the world's leading publisher of Open Access books Built by scientists, for scientists

6,900

Open access books available

186,000

International authors and editors

200M

Downloads

Our authors are among the

154

Countries delivered to

TOP 1%

most cited scientists

12.2%

Contributors from top 500 universities



WEB OF SCIENCE™

Selection of our books indexed in the Book Citation Index
in Web of Science™ Core Collection (BKCI)

Interested in publishing with us?
Contact book.department@intechopen.com

Numbers displayed above are based on latest data collected.
For more information visit www.intechopen.com



Robust Nonlinear Control Strategy for Small Wind Turbines: A Case Study

Ridha Cheikh and Hocine Belmili

Abstract

This chapter presents a case study of robust nonlinear control strategy using nonlinear feedback control technique based on Lyapunov theory and associated with robust control laws. The proposed approach aims to enhance robustness of the wind turbine control scheme. In fact, we selected as a case study, the most used electrical generator in small-scale wind applications, the Permanent Magnet Synchronous Generator (PMSG). Indeed, the control strategy presented in this chapter allows an efficient operation of the wind turbine in the standalone operating mode, offers a nonlinear handling of the WECS(s) and guarantees maximum wind power harvesting and robustness against critical working conditions. Talking about stability, in several wind generator control schemes; a such classical PI controllers-based scheme can easily be disturbed by any uncertainty of the system parameters, thus, in this chapter, we focused on how to overcome this issue by proposing a robust control strategy based on nonlinear controller derived from the Lyapunov Theory. The chapter presents numerical simulations within Matlab/SIMULINK environment. These results proved the effectiveness and the benefits of the proposed approach.

Keywords: WECS, PMSG, eigenvalues, nonlinear feedback control, Lyapunov theory, robust control

1. Introduction

During the last decade, the world has known a significant increase in electricity production from renewable energy sources, due in part to the liberalization of the electricity market, which has attracted the greed of new producers who are oriented towards cheaper productions (cogeneration, biomass, wind, etc.) and not in overly heavy investments (thermal power plants), and, secondly, because the emerging ecological awareness on climate change due to the emission of greenhouse gases has resulted in a political will that results from international protocols, such as Kyoto 1997 and Paris 2015, to encourage the use of clean and renewable energies for electricity generation [1].

Currently, wind energy is an important part of renewable energy production. Based on statistics from the Global Wind Energy Council (GWEC), more than 50 GW of clean, emission-free wind power was installed in 2018, bringing total installations to 591 GW globally; those statistics forecast that the global installed

capacity can reach more than 817 GW by 2021 [2]. However, as the wind energy is very different from conventional sources, it is an intermittent energy source that is not continuously available for conversion into electricity and outside direct control because the used primary energy cannot be stored, it may be predictable but cannot be dispatched to meet the demand of an electric power system. Thus, the rapid growth of wind energy penetration into power systems causes many problems regarding the power flow control flexibility, which has forced many countries to revise their grid codes to ensure stable and reliable network operation. Power systems can reach very high wind penetration levels, as is the case of Denmark (42.4%), Germany (14.8%) and Spain (14.1%) [3, 4].

Nowadays the major challenge of the wind energy industry is to respect the deferent electrical grid requirements of each country; this means that power systems doest accept except a pure and balanced electrical energy comes from wind farms and in case of grid disturbances; those wind farms have to remain connected and support the grid to avoid black outs [5, 6]. As a result, the successful installation of wind turbines subject to requirements imposed by any country's energy market will not be possible without the contribution of advanced and robust control strategies [7].

Currently, wind turbine technology is almost based on two topologies: fixed speed-based topology (FST) which uses Induction Machines (IMs) and variable speed-based topology (VST) which generally uses Double Fed Induction Machines (DFIMs) or Permanent Magnet Synchronous Machines (PMSMs) [8].

However, the FST topology is recognized by many advantages such as costless and no complexity even more, nevertheless it has many disadvantages such as lower efficiency; power fluctuations in the grid due to wind gusts, short life cycle due to significant efforts undergone by its structure [9]. Thus, even the wind system complexity will increase, but VST, in which power fluctuations could be reduced and hence wind gusts can be stored as kinetic energy in large rotating masses, has been proposed to mitigate all drawbacks of FST.

In recent years, choosing the type of the electrical generator of WTs is a serious subject of several research works. This component represents the heart of a WT; it is used to produce electric power with lower cost and under variable nature of the wind speed. In the wind industry, two types of generators dominate the sector: (a) the Permanent Magnet Synchronous Generator (PMSG) with very low inertia, high volumetric torque, good efficiency and better controllability, which, furthermore, with the possibility to direct drive train, has become a serious competitor of (b) the Double Fed Induction Machines (DFIG). This latest (DFIG) is the most used in wind industry sector due to the ability to control powers flow with significantly improved yield. The DFIG can operate in different speed modes (sub-synchronous, synchronous and super-synchronous). Due to the progress of modern technologies, the use of the DFIG in large power scales seems to have become a more efficient solution for electrical energy generation whether for onshore or offshore installations [10–12].

Therefore, developing robust nonlinear control algorithms for electro-mechanical systems actuated by different types of electric machinery, emphasizing system stability and robustness, is a very essential issue [13]. Under this scope, this chapter proposes a robust nonlinear control strategy based on Lyapunov Theory of a standalone Permanent Magnet Synchronous Generator (PMSM). Therefore, the chapter is focused on the design of nonlinear control strategy using the nonlinear feedback control techniques and Lyapunov theory to guarantee robustness of the wind energy conversion systems.

Finally, based on simulation results, a general conclusion is presented in this chapter showing the performance of the proposed control strategy used for the studied wind turbine.

2. Lyapunov theory and robust control association

2.1 Lyapunov theory fundamentals

The theory introduced in the late 19th century by the Russian mathematician Alexandr Mikhailovich Lyapunov is generally the most useful approach for analyzing the stability and designing control of linear or nonlinear systems. In fact, Lyapunov's work for stability problems includes two methods: the so-called linearization method and the direct method. The linearization method draws conclusions about a nonlinear system's local stability around an equilibrium point from the stability properties of its linear approximation [14]. However, the direct method (or second method) is not restricted to local motion, and determines the stability properties of a nonlinear system by constructing a scalar "energy-like" function for the system and examining the function's time variation [15]. In other words, the direct method is a generalization of the idea that if there is some "measure of energy" in a system, then we can study the rate of change of the system's energy to ascertain stability [16]. In this chapter, we will focus on the direct method for the control scheme design.

2.1.1 Lyapunov's direct method concept

Lyapunov's direct method for stability is now referred to as the Lyapunov stability criterion and makes use of a scalar "energy-like" function $V(x)$, which has an analogy to the potential function of classical dynamics.

It can be introduced for a system $\dot{x} = f(x)$ having a point of equilibrium at $x = 0$. Consider a function $V(x): \mathbb{R}^n \rightarrow \mathbb{R}$ such that

- $V(x) = 0$ if and only if $x = 0$. $V(x) > 0$ if and only if $x \neq 0$.
- $\dot{V}(x) = \frac{d}{dt} V(x) = \sum_{i=1}^n \frac{\partial V}{\partial x_i} f_i(x) = \nabla V \cdot f(x) \leq 0$ for all values of $x \neq 0$.

For asymptotic stability, the condition $\dot{V}(x) < 0$ for $x \neq 0$ is required.

Then $V(x)$ is called a Lyapunov function and the system is stable in the sense of Lyapunov.

2.1.2 Stability of a linear system

Consider a linear system described by its state space model as follows:

$\dot{X} = AX$ (A is a finite matrix), we can say that A is asymptotically (or exponentially) stable if all its eigenvalues' real parts are negative; in other words, all the system states will converge to the vicinity of their equilibrium points [16].

The above stability condition can be verified equivalently through Lyapunov concept, using the quadratic Lyapunov function as follows:

$V = X^t P X$ with P is a symmetric positive definite matrix,

- If $X \neq 0 \rightarrow X^t P X > 0$
- then $\dot{V} = \dot{X}^t P X + X^t P \dot{X}$. Replacing the value of \dot{X} we have the following:

$$\dot{V} = X^t (A^t P + P A) X = -X^t Q X, \text{ so, } A^t P + P A = -Q$$

The stability condition is that $\dot{V} < 0$ so the matrix Q should be positive definite for some definite matrix $P = P^t$ [17].

2.2 Modeling of parametric uncertainty for AC machines

2.2.1 Resistance variation

Heating of the machine windings due to temperature increase causes an increase in stator and rotor resistances. This variation can be generally presented in the following relation:

$$R = R_0(1 + \alpha T)$$

where α is the temperature coefficient value ($\approx 4.1 \times 10^{-3}$) and T is the temperature in degree Celsius.

2.2.2 Inductance variation

The variation of the inductances is caused by the saturation of the ferromagnetic materials of the machine. The dynamics of this variation and that of currents cannot be considered slow [18].

2.2.3 Skin effect

This concerns the induction machine; in fact, the rotor bars' resistance increases with the value of the frequency of rotor currents. An increase in the frequency causes a backflow of the currents to the periphery of the bars. The variation of the resistance of the bars is calculated numerically using a finite element method [18].

In steady-state operation, that is to say in the absence of parametric disturbances, the machine parameters take nominal values.

In general, the machine parameters are subject to unknown variations resulting from the different situations in which it evolves. The variation of the resistances is directly related to the fluctuations of the temperature of the machine; whereas the variations of the inductances are related to the phenomenon of magnetic saturation. This type of disturbance is called structured uncertainty.

From above, let us express the electrical parametric variations of the machine, such as:

$$\begin{cases} R_{s,r} \rightarrow R_{s,r}^0 + \Delta R_{s,r}, L_{s,r} \rightarrow L_{s,r}^0 + \Delta L_{s,r} \\ \sigma \rightarrow \sigma^0 + \Delta \sigma, T_r \rightarrow T_r^0 + \Delta T_r \end{cases}$$

2.2.4 Global uncertainty model

For an AC machine represented by the nonlinear system below:

$$\begin{cases} \dot{x} = f(x) + g(x)u \\ y = h(x) \end{cases}$$

To globally model uncertainty of the previous system, we can rewrite it as follows:

$$\begin{cases} \dot{x} = f(x) + \Delta f(x) + (g(x) + \Delta g(x))u \\ y = h(x) \end{cases}$$

where the exact part of the plant is represented by the functions (f, g, h) , while $(\Delta f, \Delta g)$ represent the uncertain part of the system [19].

A robust control of the uncertainty is not guaranteed by the linear control law. Thus, one should design a robust law based on the Lyapunov theory to achieve an input–output stability and robustness against uncertainty [19].

3. Case study: robust control of a standalone WECS-based PMSG

3.1 System modeling

The schema of the real studied system is presented in **Figure 1(a)**. However, for simplification purposes, and due to the power electronics and local grid dynamics being much faster than other system dynamics, it will not be considered and the simplified system is presented in **Figure 1(b)** [14].

From **Figure 1(b)**, the control goal is to change the chopper equivalent resistance R_L (load) at the generator terminals in order to adjust the generator speed to its optimum value, and then the maximum power capture will be achieved.

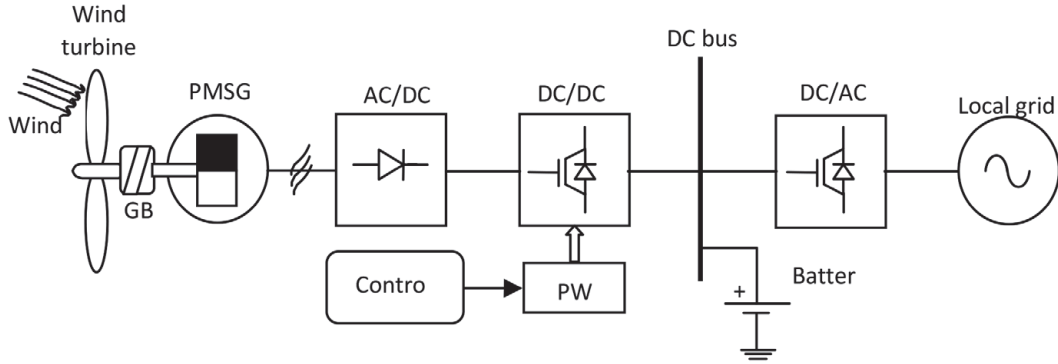
The global system model can be expressed part per part in the following equations:

$$\left\{ \begin{array}{l} v(t) = \bar{v} + \Delta v(t), \\ P_t = \Gamma_t \omega_r \\ \Gamma_t = \frac{1}{2} \pi \rho R^3 v^2 C_\Gamma(\lambda) \\ C_\Gamma(\lambda) = q_2 \lambda^2 + q_1 \lambda + q_0 \\ \lambda = \frac{\omega_r R}{v} \\ C_P = \lambda \times C_\Gamma \end{array} \right. \quad \text{Aero – mechanical part} \quad (1)$$

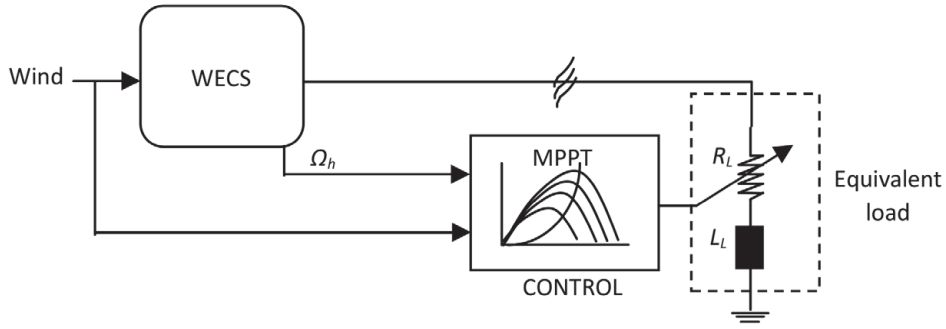
$$\left\{ \begin{array}{l} \frac{d}{dt} i_d = -\frac{R_s + R_L}{L_d + L_L} i_d + \frac{p(L_q - L_L)}{L_d + L_L} i_q \omega_h \\ \frac{d}{dt} i_q = -\frac{R_s + R_L}{L_q + L_L} i_q - \frac{p(L_d + L_L)}{L_q + L_L} i_d \omega_h + \frac{p\Phi_m}{L_q + L_L} \omega_h \end{array} \right. \quad \text{electrical part} \quad (2)$$

$$\left\{ \begin{array}{l} J_h \frac{d\omega_h}{dt} = \frac{\eta}{i} \Gamma_t - \Gamma_g \\ \omega_h = \omega_r \times i \\ \Gamma_g = p\Phi_m i_q \end{array} \right. \quad \text{Electro – mechanical part} \quad (3)$$

where $v(t)$ is the wind speed (average and turbulent components); (Γ_t, Γ_g) are respectively the turbine and generator torques; P_t is the mechanical power; (ω_r, ω_h) are turbine and generator speeds respectively; ρ is the air density; R is the swept surface radius; $C_\Gamma(\lambda)$ is the torque coefficient; (q_0, q_1, q_2) are given in the appendix; C_P is the power coefficient; λ is the tip speed ratio (TSR); η is the efficiency; i is the



(a)



(b)

Figure 1.

Schema of the studied WECS-based PMSG: (a) real system; (b) simplified system.

gearbox ratio; i_d , i_q , L_d , L_q are respectively the d/q axis currents and inductances; R_s is the stator resistance; p is the pair poles; R_L and L_L are respectively the resistance and inductance of the equivalent load.

From Eq. (1) to Eq. (3), choosing radius $x = [x_1, x_2, x_3]^T = [i_d, i_q, \omega_h]^T$ as state vector, $u = [u_1, u_2] = [R_L, v]$ as control signal and $y = \omega_h$ as a desired output, the nonlinear state space model of the system can be defined as follows:

$$\dot{x} = \begin{bmatrix} \frac{1}{L_d + L_L} (-R_s x_1 + p(L_q - L_L)x_2 x_3) \\ \frac{1}{L_q + L_L} \begin{pmatrix} -R_s x_2 - p(L_d + L_L)x_1 x_3 \\ +p\Phi_m x_3 \end{pmatrix} \\ \frac{1}{J_h} (d_3 x_3^2 - p\Phi_m x_2) \end{bmatrix} + \begin{bmatrix} -\frac{1}{L_d + L_L} x_1 u_1 \\ \frac{1}{L_q + L_L} x_2 u_2 \\ \frac{1}{J_h} (d_1 u_2^2 + d_2 u_2 x_3) \end{bmatrix} \quad (4)$$

$$\text{where } d_1 = \frac{\eta \rho \pi R^3}{2i} q_0, d_2 = \frac{\eta \rho \pi R^4}{2i^2} q_1, d_3 = \frac{\eta \rho \pi R^5}{2i^3} q_2.$$

3.2 Lyapunov linearization method

In this subsection, we will apply the Lyapunov Linearization (first method) to the studied system (Eq. (4)) in order to deal with the system's small-signal stability under wind speed variation.

Suppose that (\bar{x}, \bar{u}) is an equilibrium point and input [20].

Using Taylor's series expansion of the function f we have:

$$\begin{cases} \delta x = x - \bar{x} = [\delta x_1 \delta x_2 \delta x_3]^T \\ \delta u = u - \bar{u} = [\delta u_1 \delta u_2]^T \end{cases} \quad (5)$$

The derivative variable within a unique function can be written as:

$$\dot{x} = F(x(t), u(t)) \quad (6)$$

$$\dot{\delta}_x(t) \approx F(\bar{x}, \bar{u}) + \left. \frac{\partial F}{\partial x} \right|_{\substack{x=\bar{x} \\ u=\bar{u}}} \delta_x(t) + \left. \frac{\partial F}{\partial u} \right|_{\substack{x=\bar{x} \\ u=\bar{u}}} \delta_u(t) + \underbrace{\text{h.o.t}}_0 \quad (7)$$

where $F(\bar{x}, \bar{u}) = 0$.

Then:

$$\dot{\delta}_x(t) \approx \left. \frac{\partial F}{\partial x} \right|_{\substack{x=\bar{x} \\ u=\bar{u}}} \delta_x(t) + \left. \frac{\partial F}{\partial u} \right|_{\substack{x=\bar{x} \\ u=\bar{u}}} \delta_u(t) \quad (8)$$

The matrices, A, B of the LTI system are constant matrices:

$$A \approx \left. \frac{\partial F}{\partial x} \right|_{\substack{x=\bar{x} \\ u=\bar{u}}} \in R^n \times R^n, B \approx \left. \frac{\partial F}{\partial u} \right|_{\substack{x=\bar{x} \\ u=\bar{u}}} \in R^n \times R^m$$

The linearized version around an equilibrium point characterized by the quintuple $[\bar{x}, \bar{u}] = [\bar{i}_{sd} \bar{i}_{sq} \bar{\omega}_h \bar{R}_L \bar{v}]$ can be written as follows:

$$\dot{\delta}_x = \begin{bmatrix} a_1 + a_2 \bar{R}_L & a_3 \bar{x}_3 & a_3 \bar{x}_2 \\ b_1 \bar{x}_3 & b_2 + b_3 \bar{R}_L & b_1 \bar{x}_1 + b_4 \\ 0 & c_4 & c_2 \bar{v} + c_3 \bar{x}_3 \end{bmatrix} \delta_x + \begin{bmatrix} a_2 \bar{x}_1 & 0 \\ b_3 \bar{x}_2 & 0 \\ 0 & c_1 \bar{v} + c_2 \bar{x}_3 \end{bmatrix} \delta_u \quad (9)$$

where,

$$\begin{cases} a_1 = -\frac{R_s}{L_d + L_L}; a_2 = -\frac{1}{L_d + L_L}; a_3 = \frac{p(L_q - L_L)}{L_d + L_L}; \\ b_1 = -\frac{p(L_d + L_L)}{L_q + L_L}; b_2 = -\frac{R_s}{L_q + L_L}; b_3 = -\frac{1}{L_q + L_L}; \\ b_4 = \frac{p\Phi_m}{L_q + L_L}; c_1 = \frac{2d_1}{J_h}; c_2 = \frac{d_2}{J_h}; c_3 = \frac{2d_3}{J_h}; c_4 = -\frac{p\Phi_m}{J_h}. \end{cases}$$

3.2.1 Small-signal stability

In this section, the small-signal stability of the linearized system will be checked regarding wind speed variation; therefore, we will have a point of view about the impact of the wind speed variation on the system stability. However, in open loop, without control, the system is excited by a wide range of wind speed variation starting from the cut-in to cut-out wind speed. The eigenvalues of the matrix A (Jacobian) are calculated and presented in **Table 1**.

\bar{v} (m/s)	4	5	6	7	10	12
$\lambda_{1,2}$	$-8.56 \pm 15i$	$-7.09 \pm 18i$	$-6.29 \pm 20i$	$-5.74 \pm 23i$	$-5.07 \pm 32i$	$-4.95 \pm 37i$
λ_3	-279	-342	-406	-470	-666	-798

Table 1.
Linearized system eigenvalues under wind speed variation.

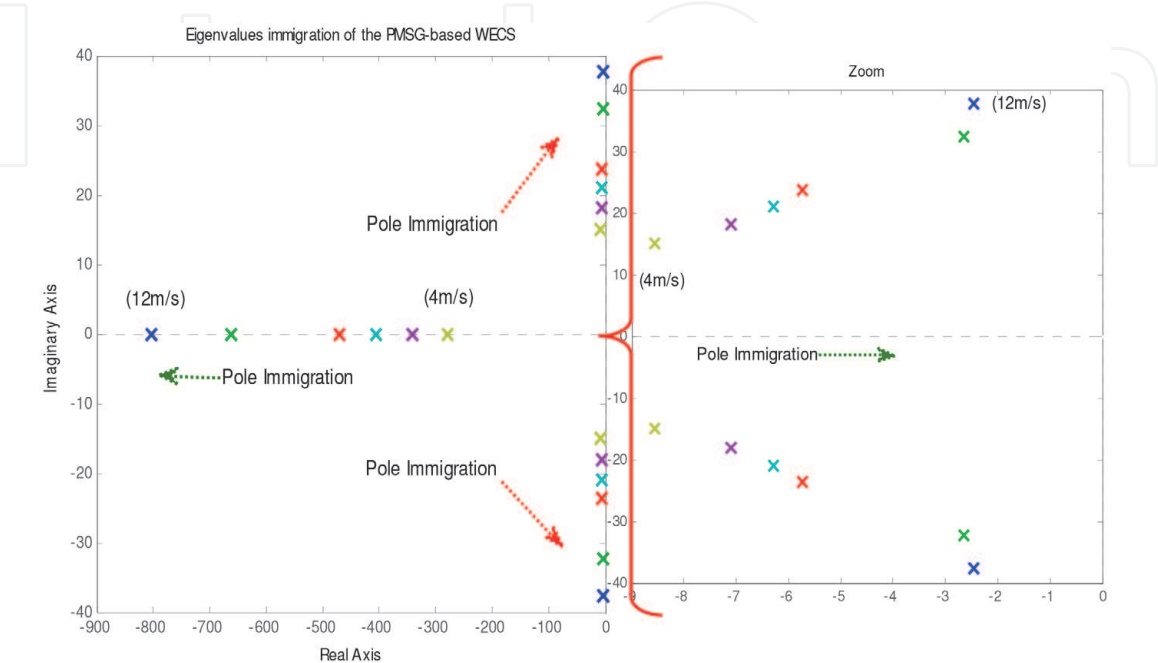


Figure 2.
Eigenvalues (poles) immigrating under wind speed variation.

Figure 2 shows clearly that for all values of wind speed, all the eigenvalues still have negative real parts and take places in the left-half of the complex plane, which means the system is almost stable under small perturbation. However, with wind speed increase, the complex-conjugated eigenvalues start immigrating almost close to the imaginary axis and then exhibit bad damping characteristics (**Figure 3**). Hence, damping should be improved in closed loop-based linear controller.

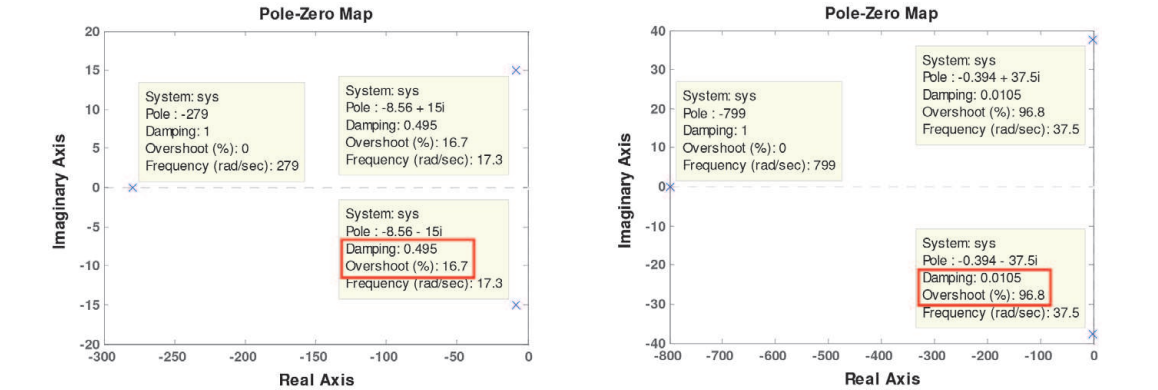


Figure 3.
System characteristics regarding damping/overshoot for two wind speed cases (4 m/s left, 12 m/s right).

3.3 System nonlinear feedback linearization

If we assume the wind speed dynamics to be very slow compared to the other system dynamics, the nonlinear system of Eq. (4) can be reformulated as follows:

$$\left\{ \begin{array}{l} \dot{x} = \underbrace{\begin{bmatrix} -\frac{R_s}{L_d + L_L}x_1 + \frac{p(L_q - L_L)}{L_d + L_L}x_2x_3 \\ -\frac{R_s}{L_q + L_L}x_2 - \frac{p(L_d + L_L)}{L_q + L_L}x_1x_3 + \frac{p\Phi_m}{L_q + L_L}x_3 \\ \frac{1}{J_h}(d_1v^2 + d_2vx_3 + d_3x_3^2 - p\Phi_mx_2) \end{bmatrix}}_{f(x)} + \underbrace{\begin{bmatrix} -\frac{1}{L_d + L_L}x_1 \\ -\frac{1}{L_q + L_L}x_2, 0 \end{bmatrix}}_{g(x)}u \\ y = h(x) = x_3 \end{array} \right. \quad (10)$$

where $d_1 = \frac{\eta\rho\pi R^3}{2i}q_0$, $d_2 = \frac{\eta\rho\pi R^4}{2i^2}q_1$, $d_3 = \frac{\eta\rho\pi R^5}{2i^3}q_2$.

The system of Eq. (10) has smooth nonlinearities; therefore, the Feedback Linearization Technique can be applied to control the system.

From Eq. (10), taking derivatives of output y with respect to time up to r times will give:

$$y^{(r)} = L_f^r h(x) + \underbrace{L_g L_f^{r-1} h(x)}_{\neq 0} u \quad (11)$$

r is the relative degree ($r < n$).

$L_f^r h(x)$ is the Lie derivative of $h(x)$ along the direction of the vector field $f(x)$ up to r times, $L_g L_f^{r-1} h(x)$ is the Lie derivative of $h(x)$ along the direction of the vector field $g(x)$.

$$\text{If we have } \begin{cases} \alpha(x) = L_f^r h(x) \\ \beta(x) = L_g L_f^{r-1} h(x) \end{cases} \quad (12)$$

Eq. (11) becomes:

$$y^{(r)} = \alpha(x) + \beta(x)u \quad (13)$$

Then the feedback linearization control can be chosen as follows:

$$u^*(x) = \frac{1}{\beta(x)}(-\alpha(x) + v) \quad (14)$$

$$y^{(r)} = v \quad (15)$$

The relative degree of Eq. (20) is $r = 2$, it is a linear input-output double-integrator, using linear methods to guarantee the system control (tracking problem).

Note that, the field vectors $\alpha(x)$ and $\beta(x)$ should be completely known to apply the feedback linearization technique [21].

The computation of the field vectors $\alpha(x)$ and $\beta(x)$ gives:

$$\begin{cases} \alpha(x) = -\frac{p\Phi_m}{J_h} [b_2x_2 + b_1x_1x_3 + b_4x_3] + \frac{1}{J_h} \left[\frac{d_2}{i}v + 2d_3x_3 \right] \dot{x}_3 \\ \beta(x) = \frac{b_4}{J_h} x_2 \end{cases} \quad (16)$$

To harvest the maximum wind power, the generator should be running at optimal speed for each wind speed, thus the generator speed reference can be expressed as follows:

$$y_r(t) = \omega_h^* = \frac{\lambda^* i v(t)}{R} \quad (17)$$

where λ^* is the optimal tip speed ratio.

Let us take an output tracking error as follows:

$$e(t) = y_r(t) - y(t) \quad (18)$$

and introduce the following error vector:

$$\xi(t) = [e(t) \ \dot{e}(t)]^T \quad (19)$$

Hence, the control objective can be achieved using the ideal control law:

$$u^*(x) = \frac{1}{\beta(x)} \left(-\alpha(x) + y_r^{(2)}(t) - k^T \xi \right) \quad (20)$$

The polynomial $s^2 + k_1s + k_2$ would have all its roots in the left-half of the complex plane if we choose an appropriate gain matrix $k = [k_2 \ k_1]^T$. This means that the tracking error asymptotically converges to zero ($\ddot{e}(t) + k_1\dot{e}(t) + k_2e(t) = 0$). Thus, the system poles are placed following the specifications concerning the overshoots and the settling times.

3.4 Robust control law design

As we mentioned previously, AC machines are subject to a large model uncertainty due to parameter variations, noises, measurement errors etc. In this chapter, we will take into account just electrical and mechanical parametric uncertainties. In the studied case, it is clear that a successful control strategy of the WECS-based PMSG hinges on the good computing of control u , which is strongly dependent on the machine parameters (Eq. (20)). Therefore, we propose a novel robust control law to handle the uncertainty issue and offer an accurate description of the system model [19].

From Section 2.2.1, Eq. (10) can be rewritten as follows:

$$\begin{cases} \dot{x} = f(x) + \Delta f(x) + (g(x) + \Delta g(x))u \\ y = h(x) \end{cases} \quad (21)$$

However, the exact parts of the model are $f(x)$, $g(x)$ and $h(x)$, while Δf and Δg present the uncertainty.

Consequently, we have:

$$\begin{cases} \ddot{y} = v + \Delta v \\ \Delta v = \Delta\alpha(x) + \Delta\beta(x)u \end{cases} \quad (22)$$

Δv is the effect of uncertainty, it is an unknown term, which makes the linear feedback control law of Eq. (15) incapable of providing a robust tracking performance of the system. Thus, the following robust control law is proposed to handle this issue.

From Eq. (22), we rewrite the error dynamics as follows:

$$\dot{\xi} = \underbrace{\begin{bmatrix} 0 & 1 \\ -k_2 & -k_1 \end{bmatrix}}_{A_c} \xi + \underbrace{\begin{bmatrix} 0 \\ 1 \end{bmatrix}}_B (v + \Delta v) \quad (23)$$

We chose the Lyapunov function as follows:

$$V = \frac{1}{2} \xi^T P \xi \quad (24)$$

The derivation of V gives

$$\dot{V} = \frac{1}{2} [\dot{\xi}^T P \xi + \xi^T P \dot{\xi}] \quad (25)$$

P is a positive semi-definite matrix in which

$$A_c^T P + P A_c = -Q \quad (26)$$

Q is an identity matrix.

After computation, \dot{V} becomes

$$\dot{V} = -\frac{1}{2} \xi^T Q \xi + \xi^T P B (v + \Delta v) \quad (27)$$

V satisfies the condition $\dot{V} < 0$ along the solution trajectory of the system, which gives the following:

$$\xi^T P B (v + \Delta v) < 0 \quad (28)$$

v is chosen as

$$v = -F \operatorname{sgn}(\xi^T P B) \quad (29)$$

with $F > |\Delta v|$.

The substitution of Eq. (29) in Eq. (28) gives

$$\xi^T P B (-F \operatorname{sgn}(\xi^T P B) + \Delta v) < 0 \quad (30)$$

Eq. (30) is always negative for any value of $\xi^T P B$ provided $F > |\Delta v|$. The value of the gain F is chosen accordingly by trial and error.

We have

$$\operatorname{sgn}(\xi^T P B) = \begin{cases} 1 & \text{if } \xi^T P B > 0 \\ 0 & \text{if } \xi^T P B = 0 \\ -1 & \text{if } \xi^T P B < 0 \end{cases} \quad (31)$$

After computation, the P matrix element can be set as follows:

$$P = \begin{bmatrix} \frac{K_1}{2K_2} + \frac{1+K_2}{2K_1} & \frac{1}{2K_2} \\ \frac{1}{2K_2} & \frac{1+K_2}{2K_1K_2} \end{bmatrix} \quad (32)$$

Finally, the linear control signal is expressed as

$$v = y_r^{(2)}(t) - k^T \xi - F \operatorname{sgn} \left(\begin{bmatrix} \frac{1}{2K_2} & \frac{1+K_2}{2K_1K_2} \end{bmatrix} \xi \right) \quad (33)$$

4. Simulation results and discussion

Based on the control scheme shown in **Figure 4**, we have simulated within Matlab/Simulink® the studied system shown in **Figure 1**. The system data are given in the appendix. Through simulation, we have considered that all system variable states (x_1, x_2, x_3) are available for feedback. The simulation aims to check two control performances, a wind maximum power tracking performance under a realistic wind speed, and robustness performance against both rapid wind speed variation (sharp) and parametric uncertainty of the generator inertia.

4.1 Tracking performance check

For tracking performance under wind speed fluctuations (**Figure 5(a)–(d)**), the power coefficient C_p holds easily its maximum value (C_{pmax}) and the same for tip speed ratio, TSR (λ^*). Consequently, the PMSG runs at optimal speeds for each wind speed value (see **Figure 5(d)**) and the maximum power extraction is indeed guaranteed (**Figure 6(b)**).

However, from **Figure 6(a)**, it should be mentioned that the control signal, which represents the equivalent chopper resistance (R_L), has the chattering phenomenon due to discontinuous control effect (see Eq. (33)). From **Figure 6(c)** and **(d)**, all system operating points are in the neighborhood of the optimal operating points.

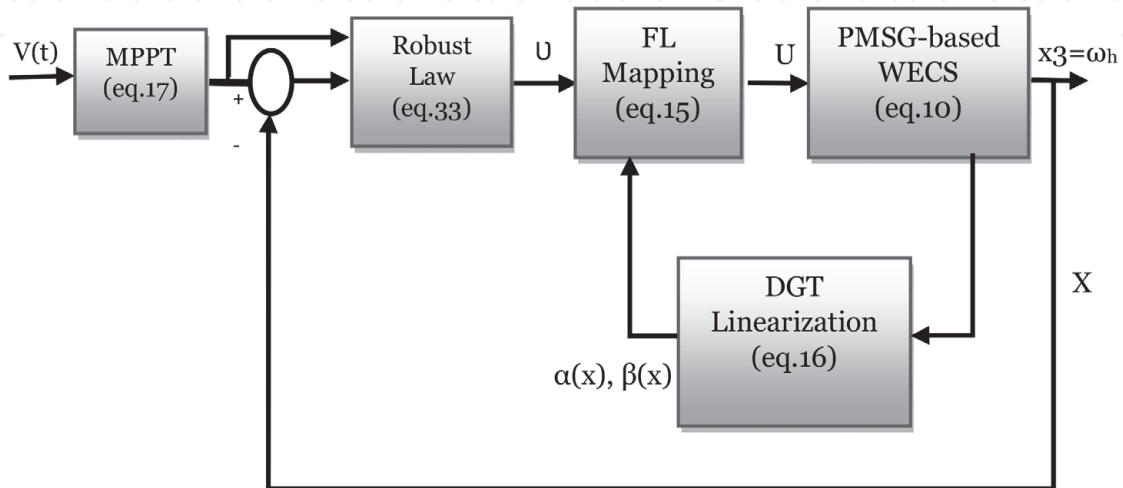


Figure 4.
Robust control simulation scheme.

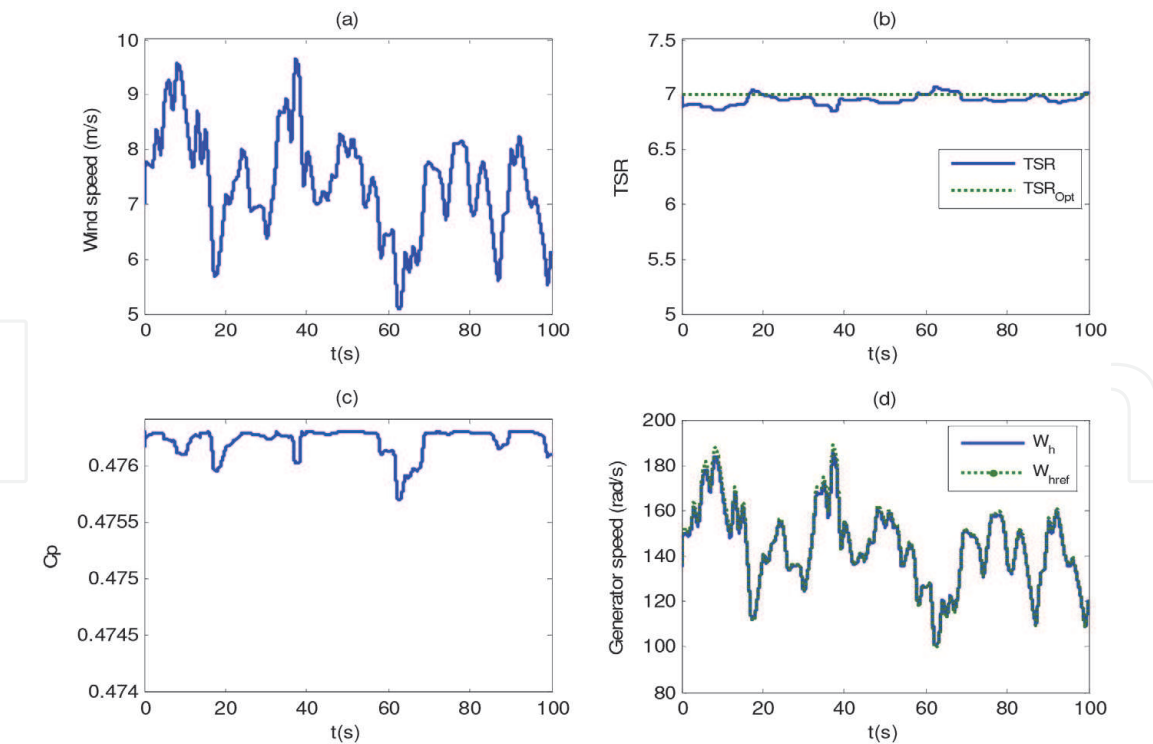


Figure 5.
Check of tracking performance under a realistic wind speed. (a) Wind speed; (b) TSR; (c) power coefficient; (d) generator speed.

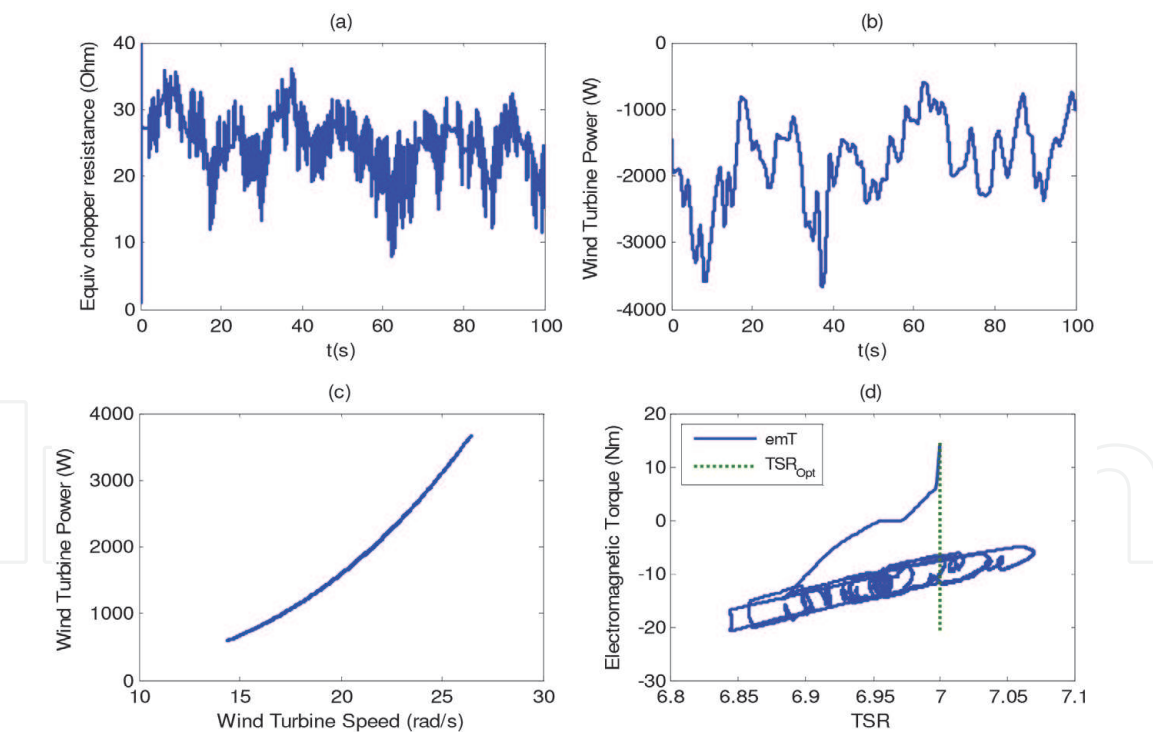


Figure 6.
(a) Control signal; (b) turbine power; (c) optimal points neighborhood; (d) electromagnetic torque versus TSR.

Then, the next simulation is to check the performance of the proposed controller facing critical wind speed conditions. Hence, we have subjected the system to a sharp rise and drop variation of the wind speed (**Figure 7(a)**). The simulation results show that even under abrupt changes of the wind speed, the system kept its stability and continued working after some short transitory disturbances and small static errors, which can be observed through **Figure 7(a)-(c)** and **Figure 8(a)-(c)**.

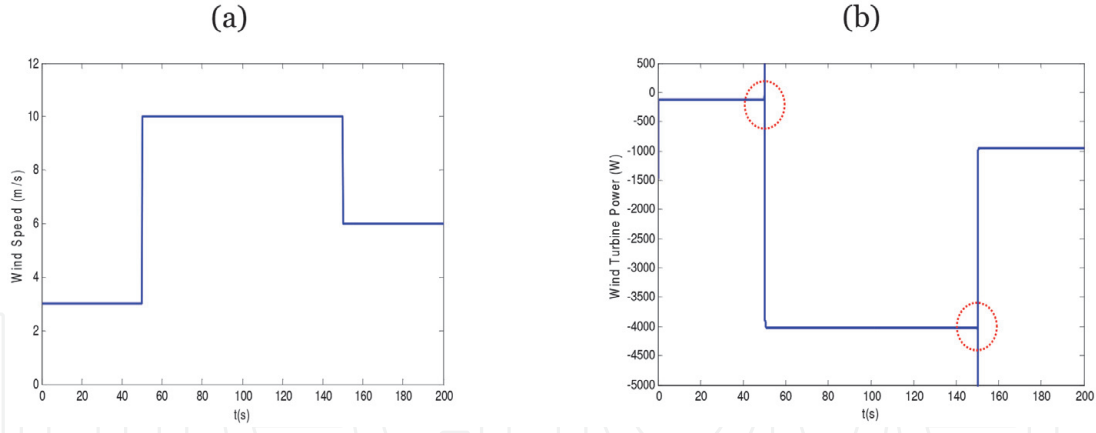


Figure 7. Robustness check under sharp wind speed variation. (a) Wind speed profile; (b) wind turbine electrical power.

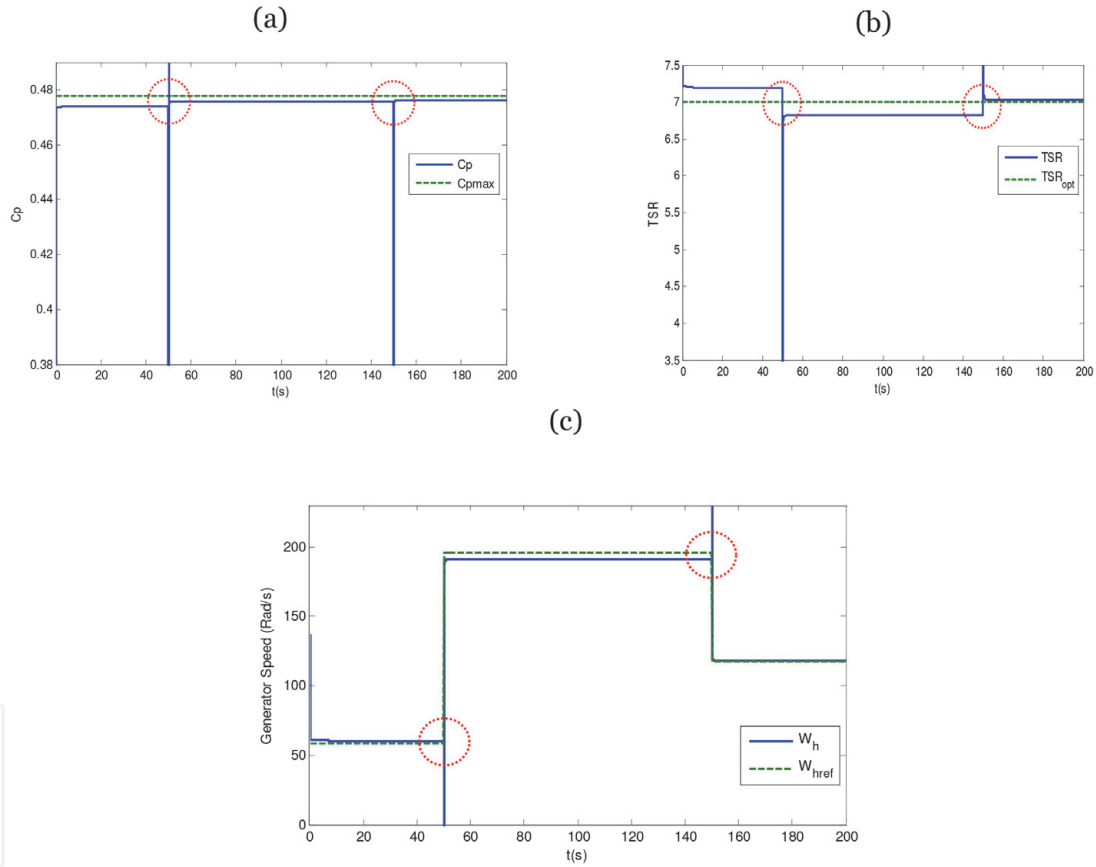


Figure 8. (a) Power coefficient; (b) tip speed ratio; (c) generator speed.

4.2 Parametric uncertainty robustness check

Following Eq. (14) and Eq. (16), it is obvious that the control signal is calculated based on field vectors $\alpha(x)$ and $\beta(x)$ whose values are strongly dependent on the system parameters, especially the high speed shaft inertia J_h . Thus, in order to check the proposed controller robustness against this parametric uncertainty, we have simulated the system with sharp variation of high speed shaft inertia as shown in **Figure 9(a)**. From the obtained simulation results (**Figures 10 and 11**), except small static errors and very small disturbances, this parametric uncertainty would not

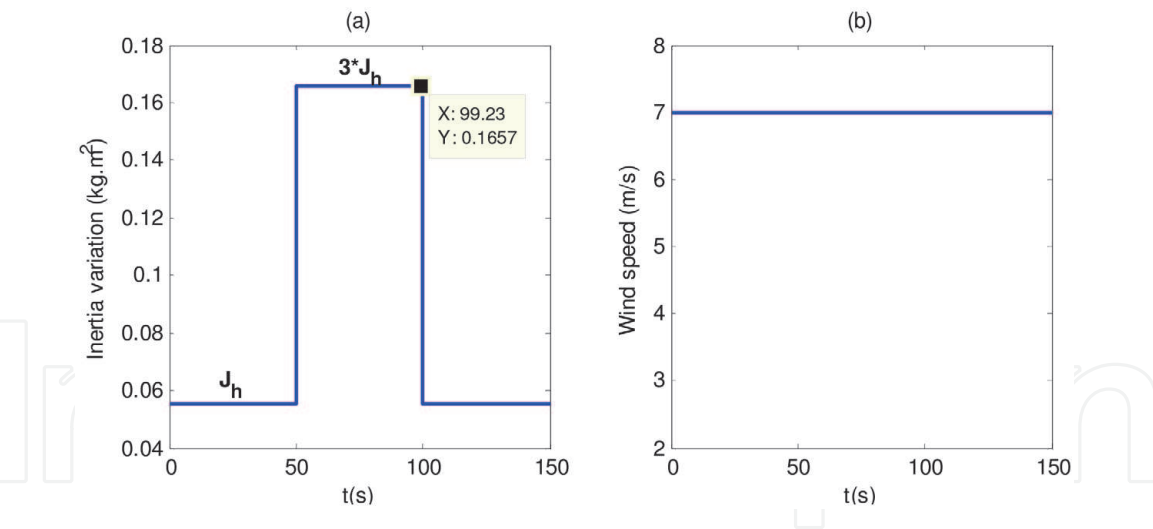


Figure 9.
(a) High speed shaft inertia; (b) average wind speed.

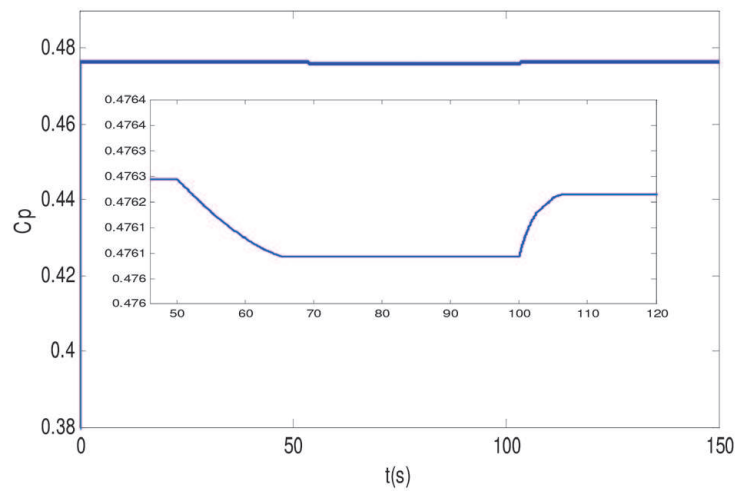


Figure 10.
Power coefficient C_p .

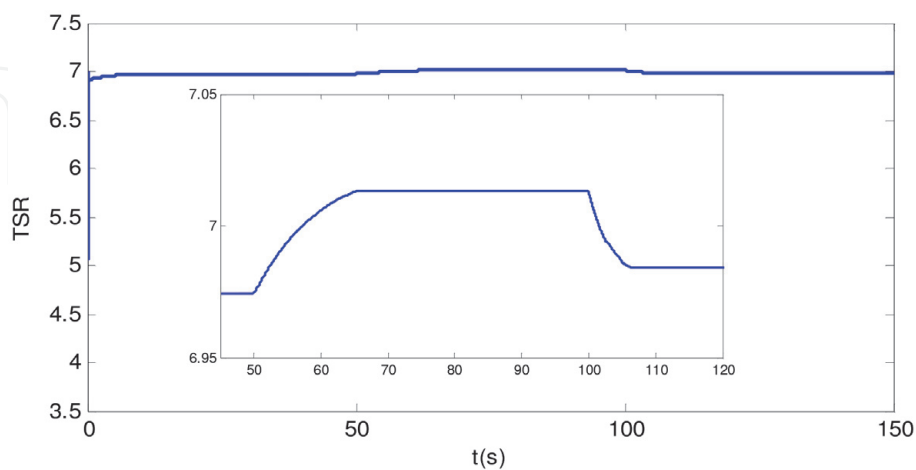


Figure 11.
Tip speed ratio.

have any notable effect on the stability of the control scheme. However, the field vectors $\alpha(x)$ and $\beta(x)$ dynamics, the control signal and the generator speed can be shown in and **Figure 12**.

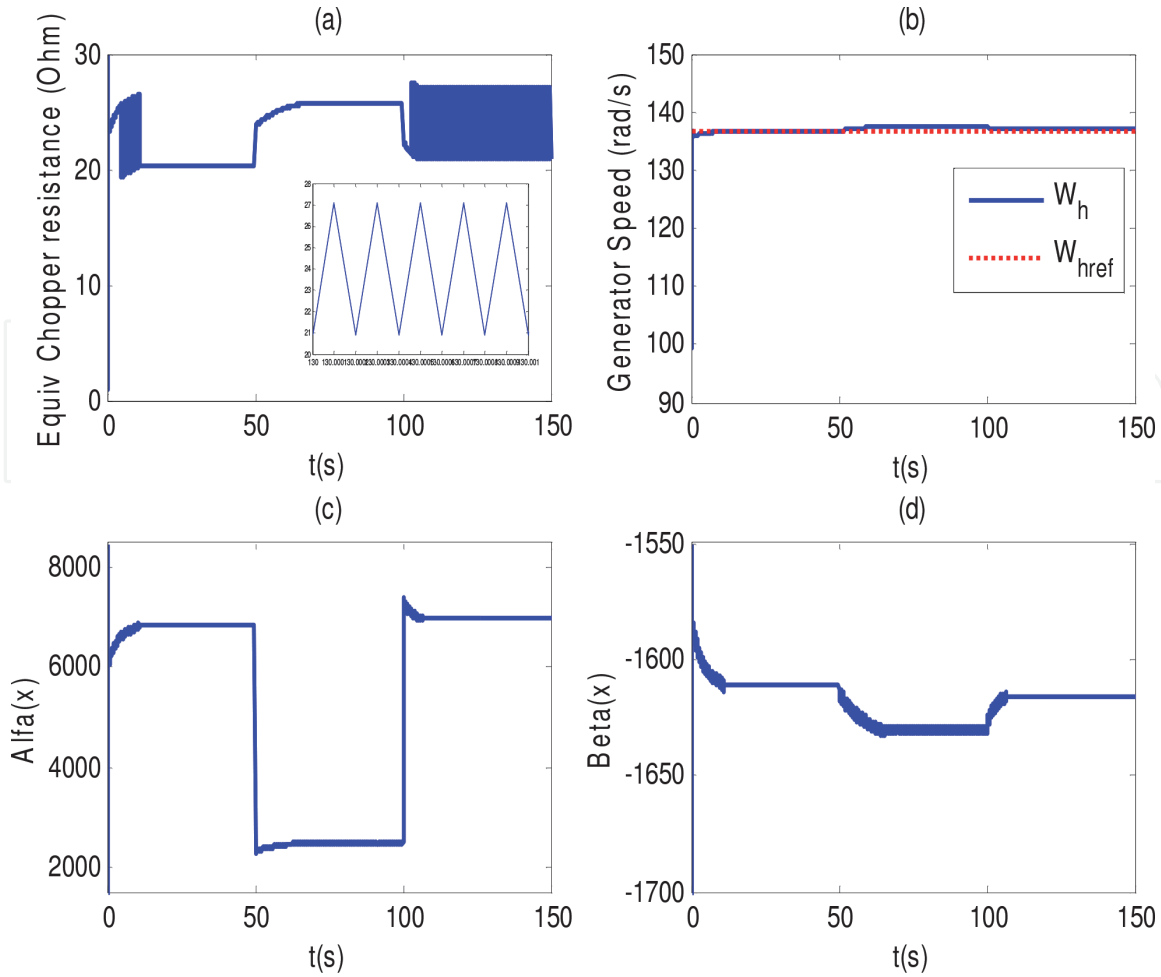


Figure 12.
 (a) Control signal; (b) generator speed; (c) $\alpha(x)$; (d) $\beta(x)$.

5. Conclusion

In this chapter, we have discussed the robust control technique based on Lyapunov theory to ensure tracking performance and robustness of a nonlinear system. Mainly, the chapter presents this control strategy based on a case study of a standalone nonlinear WECS-based PMSG. In fact, we focused on tracking performance to ensure maximum wind power extraction and robustness performance against parametric uncertainty. Whereas, the control strategy uses the state feedback linearization technique associated with a control law derived from the Lyapunov theory. The obtained results through simulation have proved the efficiency of the proposed control technique.

Appendix

Turbine rotor:

$$R = 2.5 \text{ m } \rho = 1.25 \text{ kg/m}^3, C_{Pmax} = 0.477, \lambda^* = 7$$

Drive train:

$$\eta = 1, i = 7; J_h = 0.0552 \text{ kg m}^2$$

Torque coefficient parameters:

$$q_0 = 0.0061, q_1 = -0.0013, q_2 = -9.7477 \times 10^{-4}$$

PMSG:

$p = 3, R_s = 3.3 \, \Omega$
 $L_d = 0.0416 \, \text{H}$
 $L_q = 0.0416 \, \text{H}$
 $L_L = 0.08 \, \text{H}$
 $\Phi_m = 0.4382 \, \text{Wb}$
 $V_s = 380 \, \text{V}$

Control parameters


Linear control: $k_1 = 100, k_2 = 4000$
Robust control: $F = 5000$.

Author details

Ridha Cheikh* and Hocine Belmili
Unité de Développement des Equipements Solaires, UDES, Centre de
Développement des Energies Renouvelables, CDER, Tipaza, Algeria

*Address all correspondence to: cheikh_red@yahoo.fr

IntechOpen

© 2020 The Author(s). Licensee IntechOpen. Distributed under the terms of the Creative Commons Attribution - NonCommercial 4.0 License (<https://creativecommons.org/licenses/by-nc/4.0/>), which permits use, distribution and reproduction for non-commercial purposes, provided the original is properly cited. 

References

- [1] Available from: <https://unfccc.int/resource/bigpicture/#content-the-paris-agreement>
- [2] Global Wind Energy Council (GWEC). Global wind statistics. Report 2018. 2018. Available at: www.gwec.net [Accessed: April 2019]
- [3] Flynn D et al. *Advances in Energy Systems, Technical Impacts of High Penetration Levels of Wind Power on Power System Stability: The Large-scale Renewable Energy Integration Challenge*. 1st ed. John Wiley & Sons Ltd; 2019. DOI: 10.1002/9781119508311.ch3
- [4] Wind Europe. 2019. Available at: <https://windeurope.org/about-wind/daily-wind/>
- [5] Geng H et al. LVRT capability of DFIG-based WECS under asymmetrical grid fault condition. *IEEE Transactions on Industrial Electronics*. 2013;**60**(6): 2495-2409
- [6] Shuai Xiao, Hong lin Zhou. An LVRT control strategy based on flux linkage tracking for DFIG-based WECS. *IEEE Transactions on Industrial Electronics*. 2013;**60**(7):2820-2832
- [7] Gupta A, Shandilya A. Challenges of integration of wind power on power system grid: A review. *International Journal of Emerging Technology and Advanced Engineering*. 2014;**4**(4): 880-884
- [8] Poitier F. Study and control of asynchronous generator for the use of wind energy-stand-alone induction machine-grid-connected double fed induction machine [PhD thesis]. Polytechnic School of the University of Nantes; 2003
- [9] El Aïmani S. Modeling of different wind turbine technologies integrated into a medium voltage network [PhD thesis]. École Centrale of Lille; 2004
- [10] Abad G et al. *Doubly Fed Induction Machine Modeling and Control for Wind Energy Generation*. 1st ed. IEEE-John Wiley & Sons, Inc.; 2011
- [11] Pena R et al. Doubly fed induction generator using back-to-back PWM converters and its application to variable-speed wind-energy generation. *IEE Proceedings—Electric Power Applications*. 1996;**143**(3):231-241
- [12] Cheikh R et al. Robust nonlinear control via feedback linearization and Lyapunov theory for permanent magnet synchronous generator-based wind energy conversion system. *Frontier in Energy*. 2018;**12**(46):1-12
- [13] Dawson DM et al. *Nonlinear Control of Electric Machinery*. 1st ed. UK: Taylor & Francis Group; 1998. DOI: 10.1201/9780203745632
- [14] Munteanu I et al. *Optimal Control of Wind Energy Systems: Toward a Global Approach*. UK: Springer-Verlag London Limited; 2008
- [15] Slotine JJE, Li W. *Applied Nonlinear Control*. New Jersey: Prentice-Hall, Inc.; 1991
- [16] Murray RM, Li Z, Sastry SS. *A Mathematical Introduction to Robotic Manipulation*. CRC Press; 1993
- [17] Abdelmalek G. *Commande Robuste d'un Dispositif FACTS par les Méthodes Métaheuristiques pour la Stabilité de Tension d'un Réseau Electrique* [thesis]. Department of Electrical Engineering, Biskra University University; 2019
- [18] Penman J, Sedding HG, Lloyf BA, Fink WT. Detection and location of interturns short circuits in the stator

windings of operating motors. IEEE Transactions on Energy Conversion. 1994;9(4)

[19] Ridha C et al. Robust control based on the Lyapunov theory of a grid-connected doubly fed induction. *Frontiers in Energy*. 2013;7(2):191-196. DOI: 10.1007/s11708-013-0245-y

[20] Tailor MR, Bhathawala PH. Linearization of nonlinear differential equation by Taylor's series expansion and use of Jacobian linearization process. *International Journal of Theoretical and Applied Science*. 2011; 4(1):36-38

[21] Isidori A. *Nonlinear Control Systems*. 3rd ed. Berlin: Springer-Verlag; 1995